Geophysical Journal International

*Geophys. J. Int.* (2024) **237,** 1157–1173
Advance Access publication 2024 March 11
GJI Rock and Mineral Physics, Rheology

https://doi.org/10.1093/gji/ggae100

# Relating permeability and electrical conductivity in partially saturated porous media by means of the Johnson–Koplik–Schwartz characteristic length

Luong Duy Thanh [1], Damien Jougnot [2], Santiago G. Solazzi [3], Haoliang Luo,[2] Nguyen Manh Hung,[1,4,5] Nguyen Van Nghia,[1] Phan Van Do[1] and Luong Thi Thanh Huong[1]

[1] *Thuyloi University,* 175 *Tay Son, Dong Da, Hanoi, Vietnam. E-mail: thanh_lud@tlu.edu.vn*
[2] *Sorbonne Université, CNRS, EPHE, UMR* 7619 *Metis, F-*75005 *Paris, France*
[3] *Institute of Earth Sciences, University of Lausanne, Lausanne, Switzerland*
[4] *Graduate School, Phenikaa University, Hanoi* 12116*, Vietnam*
[5] *Phenikaa Institute for Advanced Study (PIAS), Phenikaa University, Yen Nghia ward, Ha Dong district, Hanoi* 10000*, Vietnam*

Accepted 2024 March 9. Received 2024 January 24; in original form 2023 September 28

## SUMMARY

In this work, we revisit the seminal concept of Johnson–Koplik–Schwartz (JKS) length $\Lambda$, that is a characteristic length representing an effective pore size which controls various transport-related properties of porous media, such as, the permeability and the electrical conductivity. We present a novel closed-form equation that predicts the behaviour of $\Lambda$ in partially saturated media, for different saturation states. Using previous models in the literature that predict the intrinsic and relative electrical conductivities under partially saturated conditions, we infer the JKS length $\Lambda$ and the electrical formation factor $F$ as functions of water saturation and properties associated with the pore-size distribution of the probed porous medium. The proposed method permits to estimate the effective permeability and the relative permeability directly from electrical conductivity measurements, thus opening new-avenues for the remote characterization of partially saturated media. We believe that this new model will prove useful for various characterization and modelling applications from reservoir ($CO_2$ or hydrogen storage) to vadose zone studies.

**Key words:** Electrical properties; Permeability and porosity; Fractals and multifractals; Hydrogeophysics.

## 1 INTRODUCTION

Permeability or hydraulic conductivity are key pore space descriptors for modelling water flow and transport processes in porous media. Under partially saturated conditions, the permeability is known to vary with water saturation and suction head or capillary pressure. If unsaturated permeability measurements can be performed in the laboratory or in the field, it can only be done at the cost of long experiments or in a fairly intrusive manner (e.g. Reynolds & Elrick 1985; Tarantino *et al.* 2008; Bachu 2013; Pini & Benson 2013). Several propositions have been published to overcome these difficulties. On the one hand, a classical approach is to use equations or algorithms, commonly referred to as pedotransfer functions (e.g. Pachepsky & van Genuchten 2011), expressing, for example relationships between the permeability and other more easily measurable properties of porous media such as texture (e.g. Alexander & Skaggs 1987; Wösten & Van Genuchten 1988; Vereecken 1995), pore or grain size distribution data (e.g. Burdine 1953; Devlin 2015; Nghia *et al.* 2021) or moisture retention data (e.g. Campbell 1974; Tomasella & Hodnett 1997). Nevertheless, pedotransfer functions are inherently imperfect because they involve simplifying processes that are not fully understood (e.g. Brown & Heuvelink 2006; Tranter *et al.* 2010). On the other hand, indirect methods have been proposed to infer the permeability using geophysical measurements, that can be more conveniently performed in the laboratory or in the field. Several geophysical methods can be used to estimate the permeability from physical observables, such as, the seismic velocity (e.g. Rubin *et al.* 1992; Prasad 2003), the electrical resistivity (e.g. Mawer *et al.* 2015; Rezaei *et al.* 2016), the spectral induced polarization (e.g. Revil & Florsch 2010; Weller *et al.* 2015) or the ground-penetrating radar data (e.g. Corbeanu *et al.* 2002; Kowalsky *et al.* 2004).

In porous soils and rocks, electrical current flow and water flow occur in the same system of pores or cracks and they are both dependent on a common set of physical properties [e.g. pore shape, pore size, connectivity, tortuosity, porosity, see Bernabé & Maineult (2015)]. Notably,

the electrical conductivity $\sigma$ (S m$^{-1}$) and permeability $k$ (m$^2$) both are dependent on the characteristic length scale of the pore space which effectively contributes to the flow of fluids (e.g. Johnson *et al.* 1986; Banavar & Johnson 1987; Revil & Cathles III 1999; Glover & Dery 2010). This characteristic length was first described in Johnson *et al.* (1986) and it is often called the JKS length $\Lambda$ (m) in the literature (e.g. Le Doussal 1989; Glover & Walker 2009). The JKS length $\Lambda$ is obtained by weighting the individual pore sizes with respect to the local electrical field. As such, $\Lambda$ controls various transport properties of porous media. Interestingly, as $\sigma$ and $k$ share common features, new models relating these parameters are of great interest for geoscience practitioners (e.g. Li & Williams 2007; Li 2011). Relationship between $k$ and $\sigma$ have been proposed using different approaches such as the critical path analysis (e.g. Friedman & Seaton 1998; Ghanbarian 2020), effective medium theory (e.g. Doyen 1988; David *et al.* 1990) or a bundle of capillaries (BOC) (e.g. Mualem & Friedman 1991). However, most of these research efforts concentrate on fully saturated media, and, thus, extensions to partially saturated porous media are needed if two or more fluids saturate the medium.

There have been attempts to determine $k$ from $\sigma$ measurements under partially saturated conditions (e.g. Urish 1981; Purvance & Andricevic 2000; Slater & Lesmes 2002; Doussan & Ruy 2009). Niu *et al.* (2015) applied a BOC to develop the $k-\sigma$ relationship in partially saturated media. From this $k-\sigma$ relationship in combination with a model for the hydraulic conductivity proposed by Mualem (1976), Niu *et al.* (2015) obtained a new model for $\sigma$ that incorporates the tortuosity factor $q$. By fitting the new model for $\sigma$ with experimental data for six soils, Niu *et al.* (2015) obtained different values of $q$. With those values, the permeability prediction from the model proposed by Mualem (1976) was shown to be greatly improved. Recently, Fu *et al.* (2023) applied a BOC model in combination with the Waxman–Smits model to develop a hydraulic-electrical conductivity relationship under partially saturated conditions. Such relationship allowed the authors to determine the hydraulic conductivity as a function of water saturation and suction head using the Brooks–Corey model. The approach proposed by Fu *et al.* (2023) was then validated by experimental data of 150 soils. However, the approaches proposed by Niu *et al.* (2015) and Fu *et al.* (2023) required a combination of the BOC with other model(s) that are not based on the same pore-scale conceptualization, making them rather complicated for permeability predictions.

To the best of our knowledge, the JKS length $\Lambda$ remains the most reliable parameter relating electrical and flow characteristics of porous media. However, it is a parameter that was derived for fully saturated porous media (e.g. Revil & Cathles III 1999; Glover & Walker 2009; Glover & Dery 2010; Thanh *et al.* 2019, 2020a; Rembert *et al.* 2020). There are only few published results on extensions of the JKS length to partially saturated conditions. For instance, Revil *et al.* (2014) established a scaling law describing the dependence of the JKS length on water saturation based on Johnson *et al.* (1986) and Pride (1994) models in combination with a volume averaging approach. More recently. Solazzi *et al.* (2020) proposed a general expression for the JKS length using the BOC under partially saturated conditions assuming a state of capillary equilibrium. Maineult *et al.* (2018) investigated the spectral induced polarization of partially saturated random tube networks and simulated evolution of the JKS length as a function of the water saturation. However, closed equations linking $k$, $\sigma$ and $\Lambda$ have, to date, never been obtained for partially saturated porous media.

In this work, we utilize the BOC model proposed by Thanh *et al.* (2020b) for $\sigma$ to derive the JKS length $\Lambda$ and the electrical formation factor $F$ as functions of water saturation. Making use of the latter, we derive expressions for the permeability $k$ and relative permeability $k_{\text{rel}}$. Additionally, we obtain a relationship between the relative electrical conductivity $\sigma_{\text{rel}}$ and the relative permeability $k_{\text{rel}}$. Finally, proposed models for $\Lambda$, $\Lambda_{\text{rel}}$, $\sigma$, $\sigma_{\text{rel}}$, $k$ and $k_{\text{rel}}$ are validated using experimental data and compared with other models available in the literature.

## 2 THEORETICAL BACKGROUND

In this section, we summarize concepts and models available in the specific literature associated with the permeability and electrical conductivity for both fully and partially saturated porous media.

### 2.1 Permeability

#### *2.1.1 Relations for fully saturated conditions*

Permeability is one of the most important transport properties of porous media. There exist many permeability models proposed in literature (e.g. Kozeny 1927; Paterson 1983; Walsh & Brace 1984; Johnson *et al.* 1986; Sahimi & Mukhopadhyay 1996; Hunt 2001; Bernabé *et al.* 2010; Daigle 2016). The readers can also see a review of permeability models given in Bernabé & Maineult (2015), for example. Among permeability models, those based on the the Kozeny–Carman (KC) relationship are most commonly used. One of the KC models is the equivalent channel model given by (Paterson 1983; Walsh & Brace 1984; Bernabé & Maineult 2015):

$$k = \frac{C r_{\text{h}}^2}{F}, \tag{1}$$

where $C$ (unitless) is a geometric factor that is stated to be 1/8 for straight, cylindrical pores and 1/12 for thin cracks (for more details, see a summary by Walker & Glover 2010), $r_{\text{h}}$ (m) is the hydraulic radius given by

$$r_{\text{h}} = 2\frac{V_{\text{p}}}{S_{\text{p}}}, \tag{2}$$

where $V_p$ ($m^3$) is the total pore volume and $S_p$ ($m^2$) is the area of the interface between the pores and the solid matrix) and $F$ (unitless) is the electrical formation factor. It is noted that the inverse of the formation factor, that is $1/F$, is a measure of the effective interconnected porosity (e.g. Revil & Cathles III 1999). According to Johnson *et al.* (1986), one could improve the KC equation by replacing the hydraulic radius $r_h$ with the JKS characteristic length $\Lambda$

$$\Lambda = 2\frac{\int_{V_p} |\mathbf{e}_b|^2 \mathrm{d}V_p}{\int_S |\mathbf{e}_b|^2 \mathrm{d}S_p}, \tag{3}$$

where $\mathbf{e}_b$ (unitless) is the local normalized electrical field in the interconnected pore space (e.g. Revil & Cathles III 1999; Bernabé *et al.* 2010). Therefore, the JKS length $\Lambda$ corresponds to the hydraulic pore radius where volume and surface contributions are weighted by the norm of the local electrical field. That means that the local electrical field gives more weight to pores which conduct strongly (the interconnected pore space) and gives less weight to pores which conduct weakly (e.g. dead ends or disconnected pores). Hence, $\Lambda$ can be called the JKS length of porous media.

Considering the JKS length as a representative scale determining the fluid transport in combination with a BOC representation, eq. (1) is can be reformulated as

$$k = \frac{\Lambda^2}{8F}. \tag{4}$$

Note that, if one does not take into account the variation of the local normalized electrical field over the interconnected pore space, then $\Lambda$ given by eq. (3) reduces to $r_h$ given by eq. (2) and, thus, eq. (4) reduces to eq. (1).

#### *2.1.2 Relations for partially saturated conditions*

As discussed by Revil *et al.* (2014), eq. (4) can be expanded to partially saturated conditions as followings

$$k(S_w) = \frac{\Lambda(S_w)^2}{8F_a(S_w)}, \tag{5}$$

where $S_w$ (unitless) is the water saturation, $\Lambda(S_w)$ and $F_a(S_w)$ are the apparent JKS length and the apparent electrical formation factor, respectively. They are given by (e.g. Revil *et al.* 2014)

$$\Lambda(S_w) = 2\frac{\int_{V_p} |\mathbf{e}_b^w|^2 \mathrm{d}V_p}{\int_S |\mathbf{e}_b^w|^2 \mathrm{d}S}, \tag{6}$$

and

$$\frac{1}{F_a(S_w)} = \frac{1}{V}\int_{V_p} |\mathbf{e}_b^w|^2 \mathrm{d}V_p, \tag{7}$$

where $\mathbf{e}_b^w$ (unitless) is the local normalized electrical field in the pore water phase and $V$ is the total volume of the considered representative elementary volume. Note that the integrals over $V_p$ and $S$ prevail in the pores that are saturated with electrolytes only. eq. (5) is used in the following sections to determine the permeability as a function of water saturation and properties of porous media.

### 2.2 Electrical conductivity

#### *2.2.1 Relations for fully saturated conditions*

The electrical conductivity of porous media $\sigma$ is a key descriptor of the associated transport properties and, thus, is pertinent for wide range of applications in reservoir engineering and petrophysics. There are various models that permit to determine $\sigma$ from the electrical conductivity of water $\sigma_w$ and microstructural properties, such as, the porosity (e.g. Archie 1942; Friedman 2005). These models rely on different approaches, such as, effective medium assumptions (e.g. Bussian 1983; Sen *et al.* 1981b), percolation theory (e.g. Hunt 2004) or the cylindrical tube model (e.g. Herrick & Kennedy 1994; Mualem & Friedman 1991). Surface conductivity at the interface between mineral surfaces and pore water can be accounted for using alternative approaches, such as, the approach of two parallel resistors (e.g. Brovelli *et al.* 2005), the effective medium approach (e.g. Bussian 1983), the theory of percolation (e.g. Ghanbarian *et al.* 2014) or the volume averaging technique (e.g. Pride 1994; Linde *et al.* 2006). One of the models for $\sigma$ under fully saturated conditions, in which the JKS length $\Lambda$ is introduced to take the surface conductivity into consideration, is given by Johnson *et al.* (1986) and Pride (1994):

$$\sigma = \frac{1}{F}\left(\sigma_w + \frac{2}{\Lambda}\Sigma_s\right), \tag{8}$$

where $\sigma_w$ ($S\,m^{-1}$) is the electrical conductivity of the pore fluid, $\Sigma_s$ (S) is the specific surface conductance at the mineral–water interface.

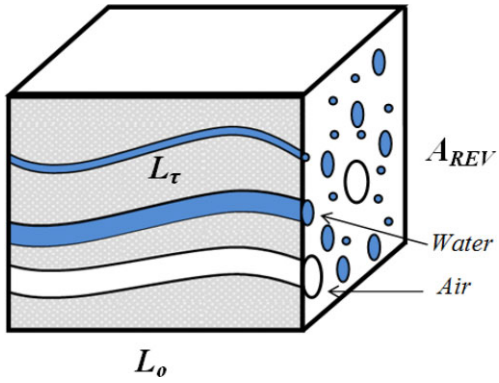


**Figure 1.** Conceptual model of a porous medium as a bundle of capillaries that is taken from Thanh *et al.* (2020b). At a given capillary pressure, capillaries are either saturated by water or by air depending on their radii.

*2.2.2 Relations for partially saturated conditions*

Revil *et al.* (2014) extended eq. (8) to partially saturated conditions

$$\sigma(S_w) = \frac{1}{F_a(S_w)}\left[\sigma_w + \frac{2}{\Lambda(S_w)}\Sigma_s\right], \tag{9}$$

where $\Lambda(S_w)$ and $F_a(S_w)$ are previously defined by eqs (6) and (7), respectively. For the case of negligible surface conductivity $\Sigma_s = 0$, eq. (9) yields

$$\sigma(S_w) = \frac{\sigma_w}{F_a(S_w)}. \tag{10}$$

## 2.3 Electrical conductivity model in fractal porous media under partially saturated conditions

In the following, we briefly describe an approach to use the fractal theory to study transport phenomena occurring in porous media. For this, we introduce the fractal electrical conductivity model proposed by Thanh *et al.* (2020b).

*2.3.1 Fractal theory for porous media*

Evidence shows that the pore space of natural porous media displays statistical self-similarity and, thus, pore sizes follow a fractal scaling law (e.g. Mandelbrot 1982; Thompson *et al.* 1987). In this context, let us conceptualize a porous medium of interest as a bundle of capillary tubes with radii varying from a minimum pore radius $r_{min}$ to a maximum pore radius $r_{max}$ (see Fig. 1; e.g. Yu & Cheng 2002; Thanh *et al.* 2019). The pore size distribution $f(r)$ is such that the number of capillaries with radius in the range from $r$ to $r + dr$ is represented by $f(r)dr$, where $f(r)$ is given by

$$f(r) = D_f r_{max}^{D_f} r^{-D_f-1} dr, \tag{11}$$

where $D_f$ (unitless) is the fractal dimension for pore space ($1 < D_f < 2$). The $D_f$ can be determined by a box-counting method (e.g. Yu & Cheng 2002). Additionally, from the approximation of self-similarity based on the Sierpinski-type gasket, $D_f$ can be estimated by (e.g. Yu & Cheng 2002):

$$D_f = 2 - \frac{\ln\phi}{\ln\alpha}, \tag{12}$$

where $\phi$ is porosity of medium and $\alpha = r_{min}/r_{max}$ is called the minimum-to-maximum pore size ratio.

The tortuous length $L_\tau(r)$ of a capillary of radius $r$ along the flow direction is normally longer than the representative length $L_o$ (see Fig. 1). Yu & Cheng (2002) proposed a relation between these two lengths by means of a fractal scaling/tortuosity relationship for flow through heterogeneous media presented by Wheatcraft & Tyler (1988) as

$$L_\tau(r) = r^{1-D_\tau} L_o^{D_\tau}, \tag{13}$$

where $D_\tau$ (unitless) is the fractal dimension for the tortuosity ($1 \leq D_\tau \leq 2$ for two dimensional spaces). $D_\tau$ can be determined by the box-counting method or by approaches based on the Monte Carlo method (e.g. Yu & Cheng 2002). In addition, $D_\tau$ can be parametrized as function of $D_f$ and $\phi$ as Wei *et al.* (2015)

$$D_\tau = (3 - D_f) + (2 - D_f)\frac{\ln\frac{D_f}{D_f-1}}{\ln\phi}. \tag{14}$$

### *2.3.2 Fractal electrical conductivity model in partially saturated media*

Based on the BOC and the above described fractal theory for porous media, Thanh *et al.* (2020b) obtained an analytical model for $\sigma$ under partially saturated conditions. This model depends on the electrical conductivity of pore water $\sigma_w$, specific surface conductance $\Sigma_s$, water saturation $S_w$, critical or residual water saturation $S_c$ and microstructural parameters of porous media such as the porosity $\phi$, $r_{min}$, $r_{max}$, $D_f$ and $D_\tau$, and it yields

$$\sigma(S_w) = \frac{\phi(3-D_\tau-D_f)}{\left(\tau_g^{eff}\right)^2(D_\tau-D_f+1)(1-\alpha^{3-D_\tau-D_f})} \left[\left\{S_w\left(1-\alpha^{3-D_\tau-D_f}\right)+\alpha^{3-D_\tau-D_f}\right\}^t - \left\{S_c\left(1-\alpha^{3-D_\tau-D_f}\right)+\alpha^{3-D_\tau-D_f}\right\}^t\right] \left[\sigma_w + \frac{2\Sigma_s}{r_{max}} \frac{(D_\tau-D_f+1)\left[1-\left\{S_c\left(1-\alpha^{3-D_\tau-D_f}\right)+\alpha^{3-D_\tau-D_f}\right\}^{\frac{D_\tau-D_f}{3-D_\tau-D_f}}\right]}{(D_\tau-D_f)\left[\left\{S_w\left(1-\alpha^{3-D_\tau-D_f}\right)+\alpha^{3-D_\tau-D_f}\right\}^t - \left\{S_c\left(1-\alpha^{3-D_\tau-D_f}\right)+\alpha^{3-D_\tau-D_f}\right\}^t\right]}\right], \tag{15}$$

where

$$t = \frac{D_\tau-D_f+1}{3-D_\tau-D_f}, \tag{16}$$

and

$$\tau_g^{eff} = \left[\frac{1-\alpha^{3-D_\tau-D_f}}{\phi}\frac{\pi D_f}{3-D_\tau-D_f}\right]^{\frac{D_\tau-1}{3-D_\tau}}. \tag{17}$$

For the case of negligible surface conductivity $\Sigma_s = 0$, eq. (15) reduces to

$$\sigma(S_w)|_{\Sigma_s=0} = \frac{\phi(3-D_\tau-D_f)\sigma_w}{\left(\tau_g^{eff}\right)^2.(D_\tau-D_f+1)(1-\alpha^{3-D_\tau-D_f})} \left[\left\{S_w\left(1-\alpha^{3-D_\tau-D_f}\right)+\alpha^{3-D_\tau-D_f}\right\}^t - \left\{S_c\left(1-\alpha^{3-D_\tau-D_f}\right)+\alpha^{3-D_\tau-D_f}\right\}^t\right]. \tag{18}$$

Thanh *et al.* (2020b) also derived an expression for the relative electrical conductivity $\sigma_{rel}$ (unitless) as a function of water saturation as

$$\sigma_{rel}(S_w) = \frac{\left\{S_w\left(1-\alpha^{3-D_\tau-D_f}\right)+\alpha^{3-D_\tau-D_f}\right\}^t - \left\{S_c\left(1-\alpha^{3-D_\tau-D_f}\right)+\alpha^{3-D_\tau-D_f}\right\}^t}{1-\left\{S_c\left(1-\alpha^{3-D_\tau-D_f}\right)+\alpha^{3-D_\tau-D_f}\right\}^t}. \tag{19}$$

In special case of zero critical water saturation $S_c = 0$ and $r_{max} >> r_{min}$ ($\alpha \to 0$) that is normally valid in geological porous media, eq. (19) reduces to

$$\sigma_{rel}(S_w)|_{\{S_c,\alpha\}\to 0} = S_w^t. \tag{20}$$

eq. (20) is identical to the power-law relationship that is commonly used in the specific literature (e.g. Jackson 2008; Ghanbarian & Sahimi 2017):

$$\sigma_{rel} = S_w^n, \tag{21}$$

where $n$ is the so-called saturation exponent (Archie 1942).

Note that using $S_c = 0$ allows reducing eq. (19) to the familiar model proposed by Jackson (2008) and Ghanbarian & Sahimi (2017). However, in real applications, especially for clay-rich porous media, the critical water saturation $S_c$ plays important role in determining the electrical properties of the porous media (e.g. Butler & Knight 1998; Titov *et al.* 2004). Even for sand samples, Titov *et al.* (2004) indicated that there is a clear transition in behaviours of chargeability and resistivity of the samples around the critical water saturation, which is related to the the water film on grain surfaces.

## 3 APPARENT FORMATION FACTOR AND JKS LENGTH

In this section, we derive closed-form analytical expressions for the apparent formation factor $F_a$ and the JKS length $\Lambda$ in partially saturated porous media. For this, we use the fractal model introduced in previous sections. Finally, we provide new relationships between $\Lambda$ and $F_a$ with the permeability and relative permeability of partially saturated porous media.

### 3.1 Apparent formation factor and JKS length

Comparing eq. (10) with eq. (18), we obtain the apparent formation factor under partially saturated conditions as

$$F_a(S_w) = \frac{\left(\tau_g^{eff}\right)^2(D_\tau-D_f+1)\left(1-\alpha^{3-D_\tau-D_f}\right)}{\phi(3-D_\tau-D_f)\left[\left\{S_w\left(1-\alpha^{3-D_\tau-D_f}\right)+\alpha^{3-D_\tau-D_f}\right\}^t - \left\{S_c\left(1-\alpha^{3-D_\tau-D_f}\right)+\alpha^{3-D_\tau-D_f}\right\}^t\right]}, \tag{22}$$

Combining eq. (9), eq. (15) and eq. (22), we obtain the JKS length under partially saturated conditions as

$$\Lambda\left(S_{\mathrm{w}}\right)=\frac{r_{\max}\left(D_{\tau}-D_{\mathrm{f}}\right)\left[\left\{S_{\mathrm{w}}\left(1-\alpha^{3-D_{\tau}-D_{\mathrm{f}}}\right)+\alpha^{3-D_{\tau}-D_{\mathrm{f}}}\right\}^{t}-\left\{S_{c}\left(1-\alpha^{3-D_{\tau}-D_{\mathrm{f}}}\right)+\alpha^{3-D_{\tau}-D_{\mathrm{f}}}\right\}^{t}\right]}{\left(D_{\tau}-D_{\mathrm{f}}+1\right)\left[1-\left\{S_{c}\left(1-\alpha^{3-D_{\tau}-D_{\mathrm{f}}}\right)+\alpha^{3-D_{\tau}-D_{\mathrm{f}}}\right\}^{\frac{D_{\tau}-D_{\mathrm{f}}}{3-D_{\tau}-D_{\mathrm{f}}}}\right]}. \tag{23}$$

eq. (22) and eq. (23) are central results of this work, as they provide simple and straightforward expressions for computing $F$ and $\Lambda$ for various saturation degrees. We remark that, to our knowledge, eq. (23) provides the first closed-form expression for the JKS length in partially saturated media in the literature.

Note that, under fully saturated conditions, $S_{\mathrm{w}}=1$, eq. (22) and eq. (23), respectively, become

$$F=F_{a}\left(S_{\mathrm{w}}=1\right)=\frac{\left(\tau_{g}^{\mathrm{eff}}\right)^{2}\left(D_{\tau}-D_{\mathrm{f}}+1\right)\left(1-\alpha^{3-D_{\tau}-D_{\mathrm{f}}}\right)}{\phi\left(3-D_{\tau}-D_{\mathrm{f}}\right)\left[1-\left\{S_{c}\left(1-\alpha^{3-D_{\tau}-D_{\mathrm{f}}}\right)+\alpha^{3-D_{\tau}-D_{\mathrm{f}}}\right\}^{t}\right]}, \tag{24}$$

and

$$\Lambda\left(S_{\mathrm{w}}=1\right)=\frac{r_{\max}\left(D_{\tau}-D_{\mathrm{f}}\right)\left[1-\left\{S_{c}\left(1-\alpha^{3-D_{\tau}-D_{\mathrm{f}}}\right)+\alpha^{3-D_{\tau}-D_{\mathrm{f}}}\right\}^{t}\right]}{\left(D_{\tau}-D_{\mathrm{f}}+1\right)\left[1-\left\{S_{c}\left(1-\alpha^{3-D_{\tau}-D_{\mathrm{f}}}\right)+\alpha^{3-D_{\tau}-D_{\mathrm{f}}}\right\}^{\frac{D_{\tau}-D_{\mathrm{f}}}{3-D_{\tau}-D_{\mathrm{f}}}}\right]}. \tag{25}$$

As suggested by Revil *et al.* (2014), $F_a(S_{\mathrm{w}})$ and $\Lambda(S_{\mathrm{w}})$ can be expressed as the product of their values at saturated conditions and those as a function of the saturation. Namely, comparing eq. (22) and eq. (24), one obtains

$$F_{a}\left(S_{\mathrm{w}}\right)=F_{a}\left(S_{\mathrm{w}}=1\right)\frac{\left[1-\left\{S_{c}\left(1-\alpha^{3-D_{\tau}-D_{\mathrm{f}}}\right)+\alpha^{3-D_{\tau}-D_{\mathrm{f}}}\right\}^{t}\right]}{\left[\left\{S_{\mathrm{w}}\left(1-\alpha^{3-D_{\tau}-D_{\mathrm{f}}}\right)+\alpha^{3-D_{\tau}-D_{\mathrm{f}}}\right\}^{t}-\left\{S_{c}\left(1-\alpha^{3-D_{\tau}-D_{\mathrm{f}}}\right)+\alpha^{3-D_{\tau}-D_{\mathrm{f}}}\right\}^{t}\right]}. \tag{26}$$

Similarly, comparing eq. (23) and eq. (25) yields

$$\Lambda\left(S_{\mathrm{w}}\right)=\Lambda\left(S_{\mathrm{w}}=1\right)\frac{\left[\left\{S_{\mathrm{w}}\left(1-\alpha^{3-D_{\tau}-D_{\mathrm{f}}}\right)+\alpha^{3-D_{\tau}-D_{\mathrm{f}}}\right\}^{t}-\left\{S_{c}\left(1-\alpha^{3-D_{\tau}-D_{\mathrm{f}}}\right)+\alpha^{3-D_{\tau}-D_{\mathrm{f}}}\right\}^{t}\right]}{\left[1-\left\{S_{c}\left(1-\alpha^{3-D_{\tau}-D_{\mathrm{f}}}\right)+\alpha^{3-D_{\tau}-D_{\mathrm{f}}}\right\}^{t}\right]}. \tag{27}$$

From eq. (27), one can define the relative JKS length as

$$\Lambda_{\mathrm{rel}}=\frac{\Lambda\left(S_{\mathrm{w}}\right)}{\Lambda\left(S_{\mathrm{w}}=1\right)}=\frac{\left[\left\{S_{\mathrm{w}}\left(1-\alpha^{3-D_{\tau}-D_{\mathrm{f}}}\right)+\alpha^{3-D_{\tau}-D_{\mathrm{f}}}\right\}^{t}-\left\{S_{c}\left(1-\alpha^{3-D_{\tau}-D_{\mathrm{f}}}\right)+\alpha^{3-D_{\tau}-D_{\mathrm{f}}}\right\}^{t}\right]}{\left[1-\left\{S_{c}\left(1-\alpha^{3-D_{\tau}-D_{\mathrm{f}}}\right)+\alpha^{3-D_{\tau}-D_{\mathrm{f}}}\right\}^{t}\right]}. \tag{28}$$

If one does not consider the variation of the length of the pores with pore size (i.e. straight parallel capillaries) and therefore, $D_{\tau}=1$ and $t=1$ as shown by eq. (16), eq. (26) and eq. (27), respectively, reduce to

$$F_{a}(S_{\mathrm{w}})|_{\{D_{\tau},\,t\}=1}=\frac{F_{a}(S_{\mathrm{w}}=1)}{S_{e}}, \tag{29}$$

and

$$\Lambda(S_{\mathrm{w}})|_{\{D_{\tau},\,t\}=1}=\Lambda(S_{\mathrm{w}}=1)S_{e}, \tag{30}$$

where $S_{\mathrm{e}}=(S_{\mathrm{w}}-S_{\mathrm{c}})/(1-S_{\mathrm{c}})$ is the effective water saturation. eq. (29) and eq. (30) are identical to the corresponding expressions proposed by Revil *et al.* (2014) when the saturation exponent $n$ is equal to 1. Note that Solazzi *et al.* (2020) also showed the relationship between $\Lambda(S_{\mathrm{w}})$ and $S_{\mathrm{w}}$ in the same manner as expected from eq. (30).

In the case of $S_{\mathrm{c}}=0$, eq. (24) and eq. (25) reduce to

$$F_{a}(S_{\mathrm{w}}=1)|_{S_{c}=0}=\frac{(\tau_{g}^{\mathrm{eff}})^{2}(D_{\tau}-D_{\mathrm{f}}+1)\left(1-\alpha^{3-D_{\tau}-D_{\mathrm{f}}}\right)}{\phi(3-D_{\tau}-D_{\mathrm{f}})(1-\alpha^{D_{\tau}-D_{\mathrm{f}}+1})}, \tag{31}$$

and

$$\Lambda(S_{\mathrm{w}}=1)|_{S_{c}=0}=\frac{r_{\max}(D_{\tau}-D_{\mathrm{f}})\left(1-\alpha^{D_{\tau}-D_{\mathrm{f}}+1}\right)}{(D_{\tau}-D_{\mathrm{f}}+1)(1-\alpha^{D_{\tau}-D_{\mathrm{f}}})}. \tag{32}$$

If $D_{\tau}=1$, eq. (31) and eq. (32) become

$$F_{a}(S_{\mathrm{w}}=1)|_{\{S_{c},\,D_{\tau}\}=0,\,1}=\frac{(\tau_{g}^{\mathrm{eff}})^{2}}{\phi}=\frac{1}{\phi}, \tag{33}$$

and

$$\Lambda(S_{\mathrm{w}}=1)|_{\{S_{c},\,D_{\tau}\}=0,\,1}=\frac{r_{\max}(1-D_{\mathrm{f}})(1-\alpha^{2-D_{\mathrm{f}}})}{(2-D_{\mathrm{f}})(1-\alpha^{1-D_{\mathrm{f}}})}. \tag{34}$$

As indicated by eq. (33), $1/F_a(S_w = 1)$ is a measure of the effective interconnected porosity (e.g. Revil & Cathles III 1999). Eq. (34) for the JKS length under fully saturated conditions has also been proposed and validated by Thanh *et al.* (2020a).

### 3.2 Permeability and relative permeability

Substituting eq. (26) and eq. (27) into eq. (5), one obtains the effective permeability under partially saturated conditions as

$$k(S_w) = \frac{\Lambda(S_w = 1)^2}{8F_a(S_w = 1)} \cdot \left\{ \frac{\left\{S_w(1-\alpha^{3-D_\tau-D_f}) + \alpha^{3-D_\tau-D_f}\right\}^t - \left\{S_c(1-\alpha^{3-D_\tau-D_f}) + \alpha^{3-D_\tau-D_f}\right\}^t}{1 - \left\{S_c(1-\alpha^{3-D_\tau-D_f}) + \alpha^{3-D_\tau-D_f}\right\}^t} \right\}^3. \tag{35}$$

The effective permeability under partially saturated conditions can be written as the product of the permeability at saturation $k_s = k(S_w = 1)$ and the relative permeability $k_{rel}$ that depends only on water saturation (e.g. Revil *et al.* 2014):

$$k(S_w) = k_s . k_{rel}(S_w). \tag{36}$$

Combining eq. (35) and eq. (36) yields the following

$$\begin{aligned} k_s &= \frac{\Lambda(S_w = 1)^2}{8F_a(S_w = 1)} \\ &= \frac{\phi r_{max}^2}{8(\tau_g^{eff})^2} \frac{(D_\tau - D_f)^2(3 - D_\tau - D_f)\left[1 - \left\{S_c(1-\alpha^{3-D_\tau-D_f}) + \alpha^{3-D_\tau-D_f}\right\}^t\right]^3}{(D_\tau - D_f + 1)^3\left[1 - \left\{S_c(1-\alpha^{3-D_\tau-D_f}) + \alpha^{3-D_\tau-D_f}\right\}^{\frac{D_\tau-D_f}{3-D_\tau-D_f}}\right]^2 (1-\alpha^{3-D_\tau-D_f})}, \end{aligned} \tag{37}$$

and

$$k_{rel}(S_w) = \left\{ \frac{\left\{S_w(1-\alpha^{3-D_\tau-D_f}) + \alpha^{3-D_\tau-D_f}\right\}^t - \left\{S_c(1-\alpha^{3-D_\tau-D_f}) + \alpha^{3-D_\tau-D_f}\right\}^t}{1 - \left\{S_c(1-\alpha^{3-D_\tau-D_f}) + \alpha^{3-D_\tau-D_f}\right\}^t} \right\}^3. \tag{38}$$

From eq. (19) and eq. (38), one can express $k_{rel}$ in terms of $\sigma_{rel}$ as follows:

$$k_{rel}(S_w) = \sigma_{rel}^3(S_w). \tag{39}$$

eq. (39) suggests a possibility to predict the relative permeability from electrical conductivity measurement for unsaturated porous media (e.g. Doussan & Ruy 2009; Revil *et al.* 2014; Niu *et al.* 2015). Please note that the boundary conditions on the pore wall are different for the fluid flow (no-slip condition) and electrical current flow (slip condition). However, these two types of flow occur in the same pore spaces (i.e. same volume/topology), and, by means of a physics-based flux average approach in Thanh *et al.* (2020b) that includes corresponding boundary conditions, we find a physically consistent macroscopic link between the fluid flow and electrical current flow.

For the case of $S_c = 0$ and $r_{max} >> r_{min}$ ($\alpha \to 0$) as proposed by Guarracino (2007) or Soldi *et al.* (2019), for example, eq. (28) and eq. (38), respectively, reduce to

$$\Lambda_{rel}(S_w) = S_w^t, \tag{40}$$

and

$$k_{rel}(S_w) = S_w^{3t}. \tag{41}$$

Combining eq. (40) and eq. (41) yields the following:

$$\Lambda_{rel}(S_w) = k_{rel}^{\frac{1}{3}}. \tag{42}$$

The similar power-law relationship between the $\Lambda_{rel}$ and $k_{rel}$ shown by eq. (42) is also observed in Maineult *et al.* (2018) $\Lambda_{rel}(S_w) = k_{rel}^{\beta}$ with $\beta = 0.154$ by simulating drainage and imbibition processes in 2D square network.

Note that eq. (41) is exactly the same as that proposed by Revil *et al.* (2014):

$$k_{rel}(S_w) = S_w^{3n}. \tag{43}$$

It is remarked that, besides the model proposed by Revil *et al.* (2014), there have been many similar models showing the relationship between the hydraulic conductivity or permeability and water saturation in the literature (e.g. Mualem 1976; Van Genuchten 1980; Fredlund & Xing 1994).

Comparing eq. (20) with eq. (21) or eq. (41) with eq. (43), one has

$$n = t = \frac{D_\tau - D_f + 1}{3 - D_\tau - D_f}. \tag{44}$$

Eq. (44) is a key relationship in this work, as it provides a direct link between hydraulic and electrical parameters by means of material properties ($D_f$ and $D_\tau$). From eq. (39), we can predict $k_{rel}$ from the electrical measurements. Additionally, from the electrical conductivity

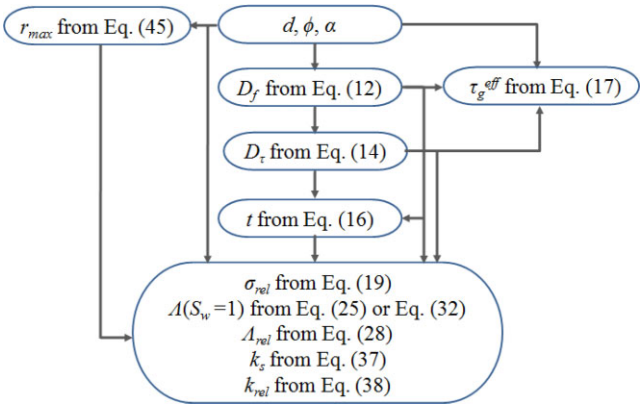


**Figure 2.** The flow chart for determination of the JKS length $\Lambda$, electrical conductivity $\sigma$ and permeability $k$ from pore fluid electrical conductivity and characteristic parameters of porous media.

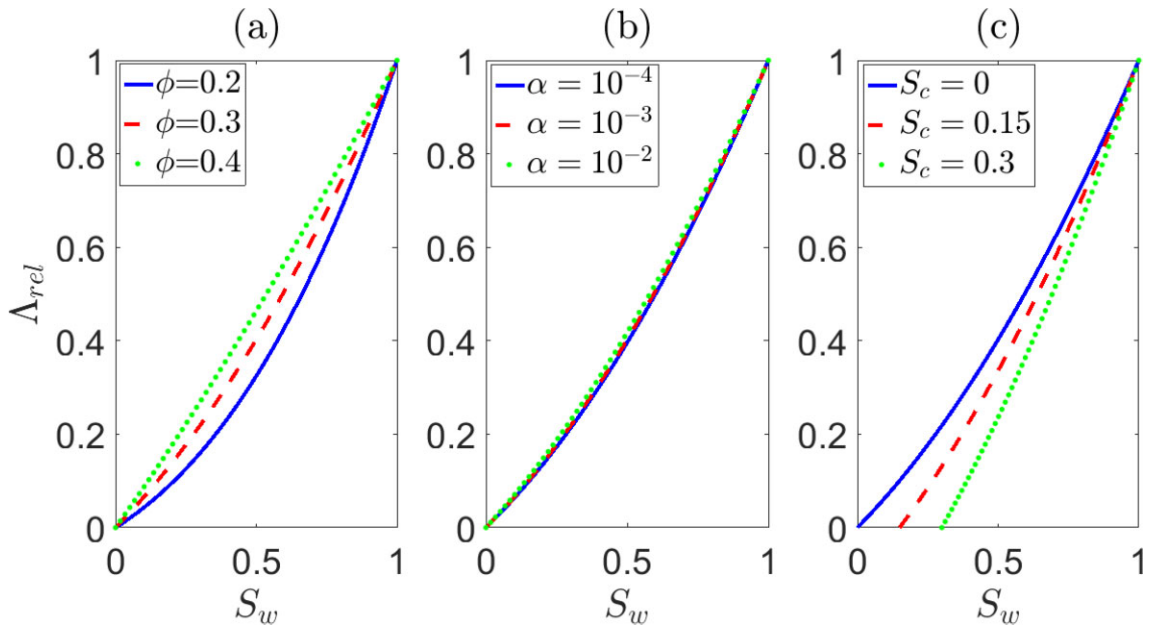


**Figure 3.** Variation of $\Lambda_{rel}$ with $S_w$ for: (a) three different values of $\phi$ (0.2, 0.3 and 0.4) at fixed values of $\alpha = 10^{-3}$ and $S_c = 0$, (b) three different values of $\alpha$ ($10^{-4}$, $10^{-3}$ and $10^{-2}$) at fixed values of $\phi = 0.3$ and $S_c = 0$ and (c) three different values of $S_c$ (0, 0.15 and 0.3) at fixed values of $\alpha = 10^{-3}$ and $\phi = 0.3$.

measurements, we can obtain $t$ from eq. (20) and substitute it into eq. (41) for the relative permeability as a function of water saturation. Please note that wettability conditions have impact on the permeability (e.g. Li *et al.* 2021) and the electrokinetic response of porous media (e.g. Collini & Jackson 2022). However, the JKS length model does not consider a slip condition at the pore walls associated with wettability effects. Consequently, these conditions are beyond the scope of this work.

## 4 SENSITIVITY ANALYSIS

In this section, we analyse the influence of the parameters $\alpha$, $\phi$, $S_c$ and $S_w$ on $\Lambda_{rel}$ and $k_{rel}$. Note that the effect of these parameters on $\sigma_{rel}$ has been presented in Thanh *et al.* (2020b). As previously shown, for given values of $\alpha$ and $\phi$, we can determine $D_f$ and $D_\tau$ from eq. (12) and eq. (14), respectively. Consequently, we can show the variation of $\Lambda_{rel}$ and $k_{rel}$ with $\alpha$, $\phi$, $S_c$ and $S_w$ from eq. (28) and eq. (38), respectively. The procedure to obtain $\Lambda_{rel}$ and $k_{rel}$ is summarized in a flow chart in Fig. 2.

The results in Figs 3 and 4 indicate the variation of $\Lambda_{rel}$ and $k_{rel}$ with $S_w$, respectively. In particular, we show the corresponding behaviours for (a) three different values of $\phi$ (0.2, 0.3 and 0.4) at fixed values of $\alpha = 10^{-3}$ and $S_c = 0$, (b) three different values of $\alpha$ ($10^{-4}$, $10^{-3}$ and $10^{-2}$) at fixed values of $\phi = 0.3$ and $S_c = 0$ and (c) three different values of $S_c$ (0, 0.15 and 0.3) at fixed values of $\alpha = 10^{-3}$ and $\phi = 0.3$. The results show that $\Lambda_{rel}$ and $k_{rel}$ increase with $S_w$ irrespective of $\phi$, $\alpha$ and $S_c$. This characteristic is in good agreement with observations reported in literature for $\Lambda_{rel}$ (e.g. Revil *et al.* 2014; Solazzi *et al.* 2020) and for $k_{rel}$ (e.g. Tuli & Hopmans 2004; Li & Horne 2006). Figs 3(a) and 4(a) show that $\Lambda_{rel}$ and $k_{rel}$ increase with $\phi$ for given values of $\alpha$, $S_w$ and $S_c$. This prediction is reasonable, due to an increase of permeability with porosity as indicated by other models (e.g. Kozeny 1927; Revil & Cathles III 1999).

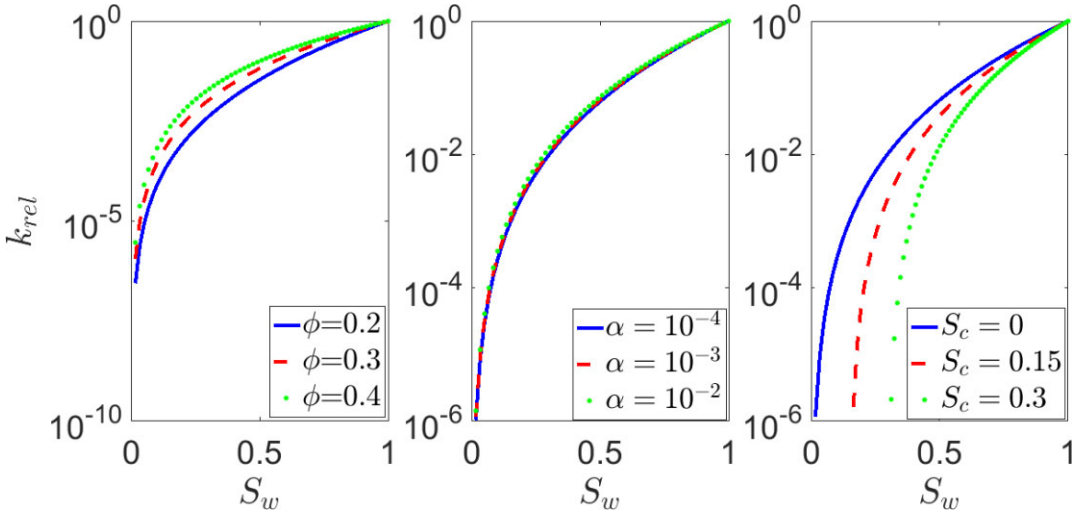


**Figure 4.** Variation of $k_{\rm rel}$ with $S_{\rm w}$ for: (a) three different values of $\phi$ (0.2, 0.3 and 0.4) at fixed values of $\alpha = 10^{-3}$ and $S_{\rm c} = 0$, (b) three different values of $\alpha$ ($10^{-4}$, $10^{-3}$ and $10^{-2}$) at fixed values of $\phi = 0.3$ and $S_{\rm c} = 0$ and (c) three different values of $S_{\rm c}$ (0, 0.15 and 0.3) at fixed values of $\alpha = 10^{-3}$ and $\phi = 0.3$.

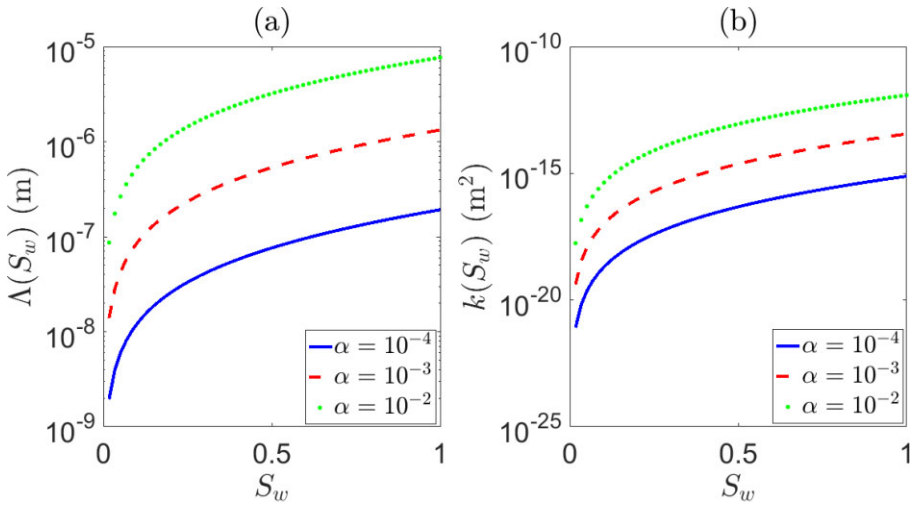


**Figure 5.** Variation of $\Lambda(S_{\rm w})$ and $k(S_{\rm w})$ with $S_{\rm w}$ at three different values of minimum-to-maximum pore size ratio $\alpha$ ($10^{-4}$, $10^{-3}$ and $10^{-2}$) for representative values of $\phi = 0.3$, $S_{\rm c} = 0$ and $r_{\rm max} = 100$ $\mu$m.

Figs 3(c) and 4(c) show that $\Lambda_{\rm rel}$ and $k_{\rm rel}$ decrease with $S_{\rm c}$ for given values of $\phi$, $\alpha$ and $S_{\rm w}$. This result is attributed to the fact that, in the context of the BOC, larger $S_{\rm c}$-values cause a reduction of the number of saturated capillaries available for water flow, which, in turn, reduces the relative JKS length and the relative permeability for a given saturation state.

Figs 3(b) and 4(b) predict that $\Lambda_{\rm rel}$ and $k_{\rm rel}$ are largely insensitive to changes in $\alpha$ at given values of $\phi$, $S_{\rm w}$ and $S_{\rm c}$. It is however noted that $\Lambda(S_{\rm w})$ and $k(S_{\rm w})$ are highly sensitive to changes in $\alpha$, as shown in Fig. 5. From eqs (23) and (35), respectively, we compute the variation of $\Lambda(S_{\rm w})$ and $k(S_{\rm w})$ with $S_{\rm w}$ at three different values of $\alpha$ ($10^{-4}$, $10^{-3}$ and $10^{-2}$) for representative values of $\phi = 0.3$, $S_{\rm c} = 0$ and $r_{\rm max} = 100$ $\mu$m (Fig. 5). The increase of $k(S_{\rm w})$ with increasing $\alpha$ predicted in Fig. 5 is in good agreement with published results (e.g. Xu & Yu 2008; Nghia *et al.* 2021).

## 5 RESULTS AND DISCUSSION

Let us now compare the proposed expressions with experimental data and previous models available in the literature. For this, estimated values for $\alpha$, $\phi$, $D_{\rm f}$, $D_\tau$, $r_{\rm max}$ and $\tau_g^{\rm eff}$ are needed. The minimum-to-maximum pore size ratio, that is $\alpha$, is optimized by searching for a minimum root-mean-square error between experimental data and predicted values. Porosity $\phi$ is readily obtained from properties of used porous samples. The fractal dimension $D_{\rm f}$ of the pore space is calculated using eq. (12) with the knowledge of $\alpha$ and $\phi$. If the pore size distribution associated with a given sample is not available to obtain $r_{\rm max}$, we proceed to predict $r_{\rm max}$ from the mean grain diameter $d$ and

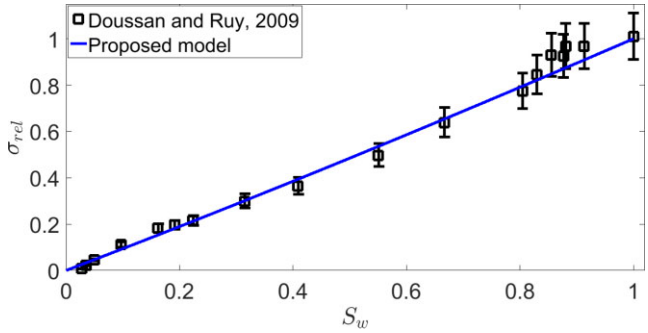


**Figure 6.** Dependence of the relative electrical conductivity $\sigma_{\text{rel}}$ on the water saturation $S_{\text{w}}$. Experimental data is taken from Doussan & Ruy (2009) for Collias loam of $\phi = 0.44$ with $\pm$ 10 per cent uncertainty. The solid line is predicted from eq. (19) with $S_{\text{c}} = 0$ Doussan & Ruy (2009) and $\alpha = 0.001$.

**Table 1.** Properties of porous samples used for estimation of $\sigma_{\text{rel}}$. Symbols $\phi, \theta_r, \alpha$ stand for the porosity, irreducible water content and the ratio of minimum and maximum radius, respectively. Superscript $^*$ stands for values reported in the corresponding references. Superscript $^{\text{f}}$ stands for values giving the best fit.

| Sample | $\phi^*$ (unitless) | $\theta_r^*$ (unitless) | $\alpha^{\text{f}}$ (unitless) | References |
|---|---|---|---|---|
| Collias loam | 0.44 | 0 | 0.001 | Doussan & Ruy (2009) |
| Sherwood sandstone | 0.4 | 0.05 | 0.001 | Amente *et al.* (2000) |
| Collias loam | 0.35 | 0.03 | 0.001 | Binley *et al.* (2002) and Dalla *et al.* (2004) |
| Sand | 0.45 | 0.06 | 0.01 | Inoue *et al.* (2000) |

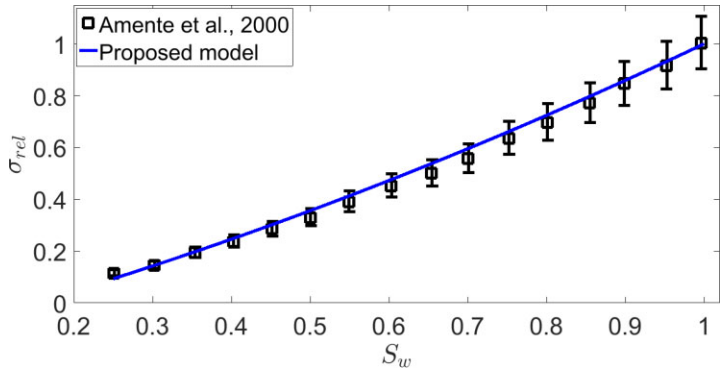


**Figure 7.** Dependence of $\sigma_{\text{rel}}$ on $S_{\text{w}}$ for Verndale Sandy loam with $\phi = 0.4$. Experimental data is taken from Amente *et al.* (2000) with $\pm$ 10 per cent uncertainty. The solid line is obtained using eq. (19) with $S_{\text{c}} = 0.15$ Amente *et al.* (2000) and $\alpha = 0.001$.

porosity $\phi$ using the following expression (e.g. Cai *et al.* 2012; Thanh *et al.* 2019):

$$r_{\max} = \frac{d}{8}\left[\sqrt{\frac{2\phi}{1-\phi}} + \sqrt{\frac{\phi}{1-\phi}} + \sqrt{\frac{\pi}{4(1-\phi)}} - 1\right]. \tag{45}$$

The fractal dimension for tortuosity $D_\tau$ is estimated from eq. (14) with known values of $D_{\text{f}}$ and $\phi$. From eq. (17), one can obtain $\tau_g^{\text{eff}}$. Finally, as described in flow chart in Fig. 2, we proceed to determine $\Lambda(S_{\text{w}})$, $\sigma(S_{\text{w}})$ and $k(S_{\text{w}})$ from the above mentioned properties and the saturation state of the probed medium.

We remark that the proposed model may be more useful for a given porous medium in real applications if parameters such as $D_{\text{f}}$, $D_\tau$, $r_{\min}$, $r_{\max}$ and $\alpha$ are fully determined in the lab. As mentioned, $D_{\text{f}}$, $D_\tau$ can be experimentally determined by the box-counting method (e.g. Yu & Cheng 2002). Additionally, $r_{\min}$, $r_{\max}$, and therefore, $\alpha$ can estimated in the laboratory by measuring the maximum capillary pressure and the air entry pressure (e.g. Ghanbarian *et al.* 2017) or from the micro-CT images and nuclear magnetic resonance measurements (e.g. Daigle 2016).

### 5.1 Relative electrical conductivity

Fig. 6 shows the variation of $\sigma_{\text{rel}}$ with $S_{\text{w}}$ for Collias loam reported by Doussan & Ruy (2009). Note that $S_{\text{w}}$ is deduced using the relation $S_{\text{w}} = \theta/\phi$, where $\phi = 0.44$ and $\theta$ is water content taken from Doussan & Ruy (2009). The solid line for $\sigma_{\text{rel}}$ is obtained using eq. (19) with $S_{\text{c}} = 0$ Doussan & Ruy (2009) and $\alpha = 0.001$ provides the best fit of the proposed model to the data (see Table 1).

Figs 7, 8 and 9 show the variation of $\sigma_{\text{rel}}$ with $S_{\text{w}}$ for Verndale Sandy loam ($\phi = 0.4$) reported by Amente *et al.* (2000), for Sherwood sandstone ($\phi = 0.35$) reported by Binley *et al.* (2002) and Dalla *et al.* (2004) and for sand ($\phi = 0.45$) reported by Inoue *et al.* (2000),

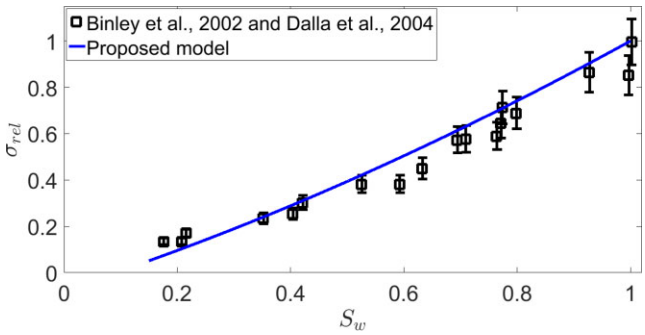


**Figure 8.** Dependence of $\sigma_{\rm rel}$ on $S_{\rm w}$ for Sherwood sandstone with $\phi = 0.35$. Experimental data is taken from Binley *et al.* (2002) and Dalla *et al.* (2004) with $\pm 10$ per cent uncertainty. The solid line is obtained using eq. (19) with $S_{\rm c} = \theta_r/\phi = 0.09$ with $\theta_r = 0.03$ Binley *et al.* (2002) and $\alpha = 0.001$.

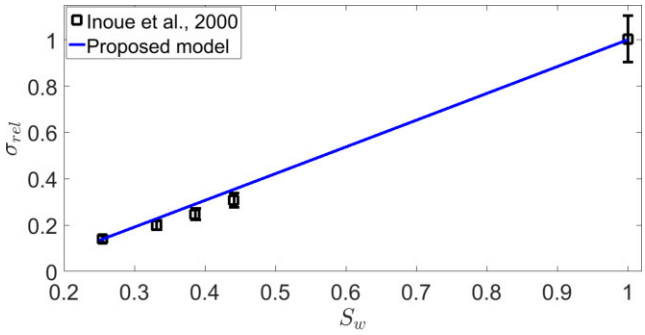


**Figure 9.** Dependence of $\sigma_{\rm rel}$ on $S_{\rm w}$ for a sand sample with $\phi = 0.45$. Experimental data is taken from Inoue *et al.* (2000) with $\pm 10$ per cent uncertainty. The solid line is obtained using eq. (19) with $S_{\rm c} = \theta_r/\phi = 0.13$ with $\theta_r = 0.06$ Inoue *et al.* (2000) and $\alpha = 0.001$.

respectively. The solid lines are predicted using eq. (19) with $S_{\rm c} = 0.15$ Amente *et al.* (2000) for Fig. 7, $S_{\rm c} = \theta_r/\phi = 0.09$ with $\theta_r = 0.03$ Binley *et al.* (2002) for Fig. 8 and $S_{\rm c} = \theta_r/\phi = 0.13$ with $\theta_r = 0.06$ Inoue *et al.* (2000). For each of these samples, used $\alpha$-values are summarized in Table 1. The comparisons of the experimental measurements with the proposed model are given in Figs 6–9, evidencing that the proposed model is able to reproduce experimental data across different soils.

### 5.2 JKS length

There exist other models in literature that allow to predict the JKS length $\Lambda$ from properties of porous media under fully saturated conditions. One of them is given by Revil & Cathles III (1999):

$$\Lambda(S_{\rm w} = 1) = \frac{d}{2m(F-1)}, \tag{46}$$

where $d$ is the mean grain diameter, $m$ is the cementation exponent and $F$ is the formation factor.

It is interesting to compare the $\Lambda$-value with that of the hydraulic radius. For a pack of uniform glass beads of diameter $d$ and porosity $\phi$, the hydraulic radius is given by (e.g. Bernabé *et al.* 2016)

$$r_{\rm h} = \frac{\phi d}{3(1-\phi)}. \tag{47}$$

Fig. 10 shows the variation of $\Lambda(S_{\rm w} = 1)$ at saturated conditions with grain diameter predicted from eq. (32) (square symbols) and from eq. (46) (diamond symbols) for a set of glass beads reported by Glover & Dery (2010). The properties of those samples are already reported by Glover & Dery (2010) is reshown in Table 2. For spherical beads, $m$ is taken as 1.5 (e.g. Sen *et al.* 1981a; Glover & Dery 2010). The approach to predict $\Lambda$ from eq. (32) is summarized in Fig. 2 where $\alpha$ is taken as 0.01, $\phi$ and $d$ are reported in Table 2. Note that a $\alpha$-value of 0.01 has been used for the same sample in Thanh *et al.* (2020a). Additionally, we also show the variation of the hydraulic radius with grain diameter predicted from eq. (47). It is seen that the proposed model provides a similar trend with those predicted from Revil & Cathles III (1999) (circle symbols) and Bernabé *et al.* (2016) (star symbols). The deviation observed in Fig. 10 can be reduced by considering the critical water saturation $S_{\rm c}$. For example, if we use eq. (25) with $S_{\rm c} = 0.15$, the model prediction is now closer to Revil & Cathles III (1999) and Bernabé *et al.* (2016) for the hydraulic radius. The reason for an increase of $\Lambda$ with the inclusion of $S_{\rm c}$ as predicted in Fig. 10 may be that pores with radii smaller than the critical pore radius that corresponds to the critical water saturation $S_{\rm c}$ are considered incapable of water flow and transport. A higher $S_{\rm c}$ value will results in a reduction in the number of saturated capillaries available for water flow, leading to a reduction of the specific surface area, thereby increasing the JKS length.

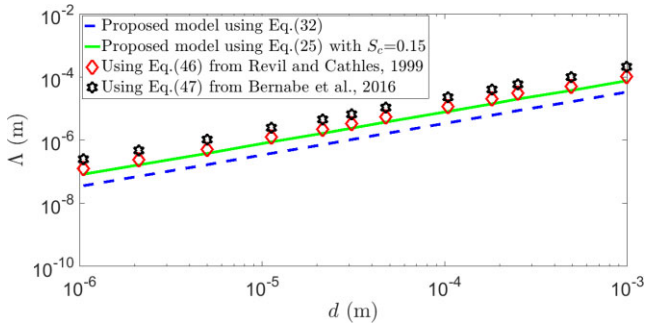


**Figure 10.** Variation of $\Lambda(S_w = 1)$ with grain diameter for a set of glass beads reported in Glover & Dery (2010) predicted from eq. (32), eq. (25) and eq. (46). The variation of the hydraulic radius with grain diameter predicted from eq. (47) is also shown for comparison.

**Table 2.** Properties of the glass beads reported by Glover & Dery (2010). Symbols $d$, $\phi$, $F$, $\alpha$ and $k_s^{exp}$ stand for the grain diameter, porosity, formation factor, ratio of minimum and maximum radius and measured permeability of samples, respectively. Superscript * stands for values reported in the corresponding references. Superscript f stands for values giving the best fit.

| Pack | $d^*$ ($\mu$m) | $\phi^*$ (unitless) | $F^*$ (unitless) | $\alpha^f$ (unitless) | $k_s^{exp*}$ ($10^{-12}$ m$^2$) |
|---|---|---|---|---|---|
| Glass bead | 1.05 | 0.411 | 3.80 | 0.01 | 0.00057 |
| Glass bead | 2.11 | 0.398 | 3.98 | 0.01 | 0.00345 |
| Glass bead | 5.01 | 0.380 | 4.27 | 0.01 | 0.0181 |
| Glass bead | 11.2 | 0.401 | 3.94 | 0.01 | 0.0361 |
| Glass bead | 21.5 | 0.383 | 4.22 | 0.01 | 0.228 |
| Glass bead | 31 | 0.392 | 4.07 | 0.01 | 0.895 |
| Glass bead | 47.5 | 0.403 | 3.91 | 0.01 | 1.258 |
| Glass bead | 104 | 0.394 | 4.04 | 0.01 | 6.028 |
| Glass bead | 181 | 0.396 | 4.01 | 0.01 | 21.53 |
| Glass bead | 252 | 0.414 | 3.75 | 0.01 | 40.19 |
| Glass bead | 494 | 0.379 | 4.29 | 0.01 | 224 |
| Glass bead | 990 | 0.385 | 4.19 | 0.01 | 866.7 |

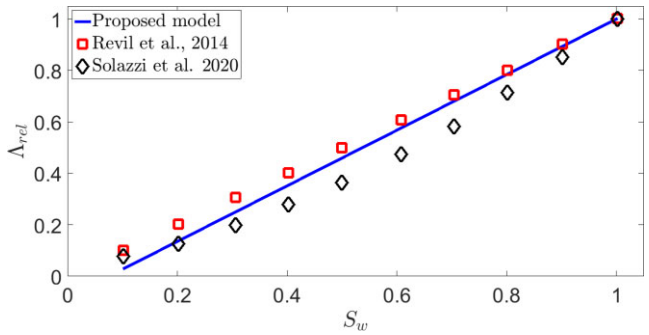


**Figure 11.** Variation of the relative characteristic length scale $\Lambda_{rel}$ with water saturation $S_w$ predicted from eq. (30), the model proposed by Revil *et al.* (2014) and data produced by Solazzi *et al.* (2020).

By fitting the dynamic permeability as a function of frequency for each saturation states deduced from the Darcy's law and Johnson *et al.* (1987) model, Solazzi *et al.* (2020) showed the variation of $\Lambda_{rel}$ with $S_w$ shown in Fig. 11 (diamond symbols) for a representative sample following the fractal pore size distribution with $D_f = 1.41$, $\alpha = 0.01$, $r_{max} = 111$ $\mu$m and $r_{min} = 1.11$ $\mu$m. The observation in Fig. 11 can be explained by eq. (30), that is, $\Lambda_{rel} = S_e$ in which $S_c$ is optimized to be 0.075. Additionally, the relation $\Lambda_{rel} = S_w$ proposed by Revil *et al.* (2014) for $n = 1$ is also used to reproduce the signature shown in Fig. 11. It is seen that eq. (30) provides a good match with the prediction by Solazzi *et al.* (2020) and Revil *et al.* (2014). Similarly, a better agreement between the proposed model with Revil *et al.* (2014) or with Solazzi *et al.* (2020) can be obtained by taking into account the critical water saturation and the variation of capillary lengths using eq. (28). However, we do not intent to carry out an exhaustive inversion of the parameters of the proposed model to find those that best fit the model Revil *et al.* (2014) or data that was synthetically reproduced by Solazzi *et al.* (2020). Our intention is to show that the proposed model is able to replicate data and other models in the literature using a rather simple closed equation.

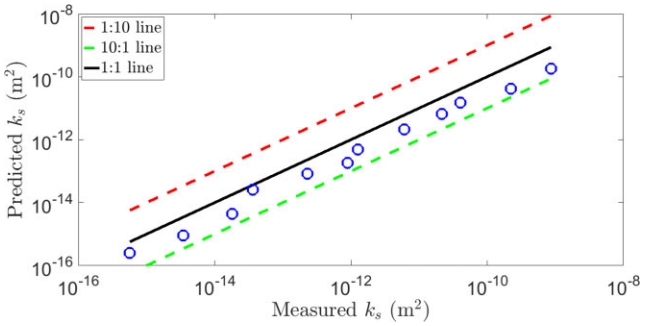


**Figure 12.** Comparison between measured permeability reported by Glover & Dery (2010) and predicted one by eq. (37). The sample properties are given in Table 2 with $S_c = 0$. The solid line is the 1:1 line. The dashed lines correspond to the 1:10 and the 10:1 ones.

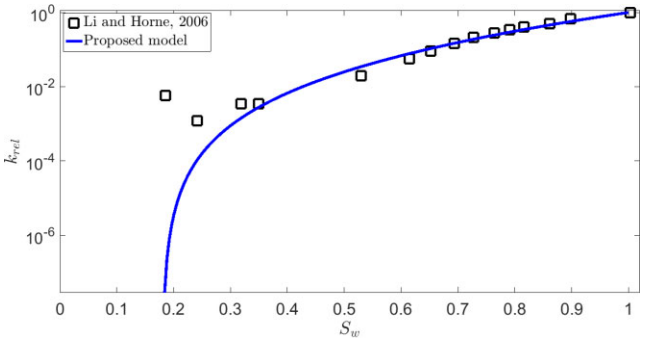


**Figure 13.** Variation of $k_{rel}$ as a function of $S_w$ for a Berea core sample reported in Li & Horne (2006) (see symbols) and predicted by eq. (38) (solid line) with $S_c = 0.18$ and $\phi = 0.25$.

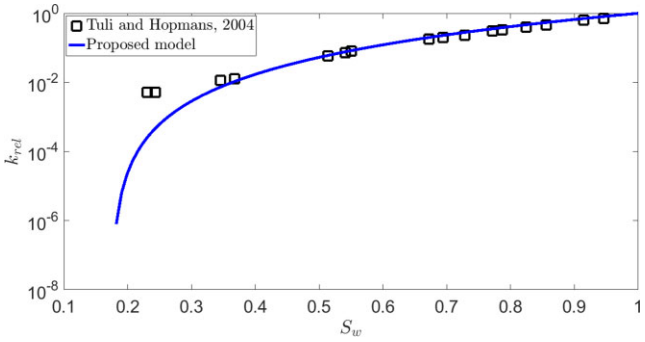


**Figure 14.** Variation of $k_{rel}$ as a function of $S_w$ for Oso Flaco fine sand reported in Tuli & Hopmans (2004) (see symbols) and predicted by eq. (38) (solid line) with $S_c = 0.17$ and $\phi = 0.42$.

### 5.3 Permeability and relative permeability

Let us now compare the fully saturated permeability $k_s$ from eq. (37) and the experimental data obtained from Glover & Dery (2010) (Fig. 12). The sample properties are summarized in Table 2. For the corresponding unconsolidated samples (e.g. sand beads, glass beads), we take $\alpha = 0.01$, which is commonly used in literature (e.g. Thanh *et al.* 2018, 2019; Solazzi *et al.* 2020; Thanh *et al.* 2020a). As seen in the flow chart of Fig. 2, from the grain diameter $d$, porosity $\phi$ and ratio $\alpha$ (see Table 2), values of $D_f$, $D_\tau$ and $r_{max}$ are obtained using eq. (12), eq. (14) and eq. (45), respectively. Then $\tau_g^{eff}$ and $t$ are obtained using eq. (17) and eq. (16), respectively. Substituting all into eq. (37), one can estimate $k_s$ at saturated conditions. In Fig. 12, we also show the 1:1 line (the solid line), the 1:10 and the 10:1 lines (the dashed lines) which act as reference lines. It is seen that the proposed model can reproduce experimental data rather well with a difference less than one order of magnitude.

Fig. 13 shows the variation of $k_{rel}$ as a function of water saturation $S_w$ for a Berea core sample measured in Li & Horne (2006), where $\phi = 0.25$ and $S_c = 0.18$ (see symbols). The observed behaviour can be reproduced by eq. (38) (see solid line) where $\alpha = 0.001$. Values of $D_f$, $D_\tau$ and $t$ are estimated based on the flow chart in Fig. 2 with the knowledge of $\phi$ and $\alpha$. Similarly, Fig. 14 shows the variation of $k_{rel}$ as a function of $S_w$ for Oso Flaco fine sand measured by Tuli & Hopmans (2004), where $\phi$ and $S_c$ were stated to be 0.42 and 0.17, respectively (see symbols). The solid line is predicted from eq. (38) with $\alpha = 0.001$. The results show that the predictions from eq. (38) are in relatively good agreement with measured data reported by Li & Horne (2006) and Tuli & Hopmans (2004) except at low water saturation, specially

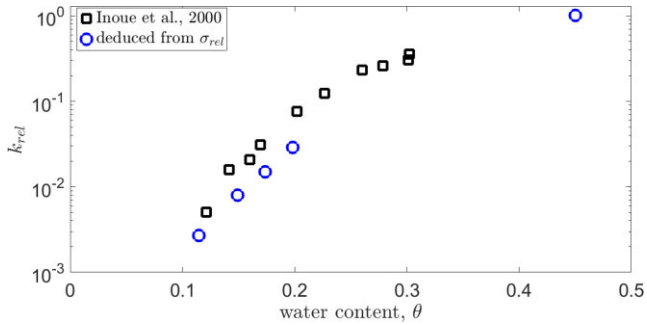


**Figure 15.** Variation of $k_{\text{rel}}$ with water content $\theta$ taken from the experimental I of Inoue *et al.* (2000) for sand (see squares). Eq. (39) is used to predict the $k_{\text{rel}}$ from $\sigma_{\text{rel}}$ for the same sample (see circles).

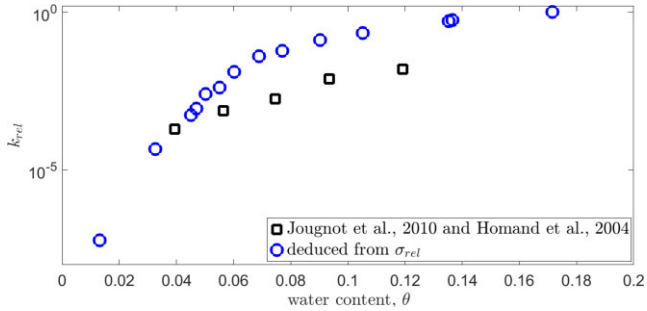


**Figure 16.** Variation of $k_{\text{rel}}$ with water content $\theta$ taken from Jougnot *et al.* (2010) and Homand *et al.* (2004) for Callovo-Oxfordian clay rock (see squares). Eq. (39) is used to predict the $k_{\text{rel}}$ from $\sigma_{\text{rel}}$ for the same sample (see circles).

close to the critical water saturation. The observed deviation possibly indicates that close to critical water saturation, there is only thin water film on grain surfaces and, consequently, applying a bundle of capillaries is no longer suitable to study transport properties in porous media.

### 5.4 Predicting permeability from electrical conductivity measurement

The variation of the $k_{\text{rel}}$ with $S_{\text{w}}$ taken from Inoue *et al.* (2000) for sand (see squares) with $\phi = 0.45$ is shown in Fig. 15. Additionally, from Fig. 9 in combination with eq. (39), we can deduce $k_{\text{rel}}$ from $\sigma_{\text{rel}}$ as shown in Fig. 15 (see circles). Similarly, Fig. 16 shows the variation of $k_{\text{rel}}$ for with $S_{\text{w}}$ for clay-rock samples from Jougnot *et al.* (2010) and Homand *et al.* (2004) as shown by square symbols (reproduced by Niu *et al.* (2015) as shown in their Fig. 11) for Callovo-Oxfordian clay rock of $\phi = 0.17$. eq. (39) is also used to predict the $k_{\text{rel}}$ from $\sigma_{\text{rel}}$ for the same sample (see circles). It is seen that eq. (39) is able to reproduce the main trend of experimental data. It suggests that the permeability could be predicted from electrical conductivity measurement for unsaturated porous media using a simple relation given by eq. (39).

### 5.5 Limitation and perspectives of the proposed model

Even though the proposed model is capable of replicating experimental data and other models in the literature using a rather simple closed equation, it comprises limitations. First, it is based on an oversimplified conceptualization of the pore probed porous medium as a bundle of capillary tubes, thus dismissing pore-space heterogeneity and dead-end pores. Therefore, it may fail to reliably replicate the response of the medium at lower water saturations due to the effect of the absorptive water. Additionally, this study only uses a relatively simple fractal pore size distribution to obtain closed and simple expressions. However, there are also different pore size distributions that can be applied to characterize a porous medium (e.g. Vinogradov *et al.* 2021).

As indicated in Roubinet *et al.* (2018), electrical current flow and water flow occur in the same systems of the pore spaces or cracks and fractures in sediments and rocks. They both rely on a common set of physical properties, such as size distribution of pores and tortuosity, connectivity, and porosity (e.g. Bernabé & Maineult 2015). Therefore, we plan to develop an analytical model for fractured media using the current approach in the near future (e.g. Guarracino & Jougnot 2022; Thanh *et al.* 2023).

## 6 CONCLUSIONS

In this work, we revisit the seminal concept of Johnson–Koplik–Schwartz characteristic length $\Lambda$ and extend its definition to partially saturated media. This characteristic length represents an effective pore size aperture that controls various transport properties such as permeability and the electrical conductivity. Using previous models in the literature that predict the intrinsic and relative electrical conductivities under partially

saturated conditions, we infer the characteristic length scale $\Lambda$, $\Lambda_{rel}$ and electrical formation factor $F$ as functions of water saturation and properties associated with the pore-size distribution of the probed porous medium. From obtained parameters, we derive expressions for the permeability $k$ and relative permeability $k_{rel}$ in partially saturated porous media. Additionally, we obtain the relationship between the relative electrical conductivity $\sigma_{rel}$ and relative permeability $k_{rel}$. Finally, we show the influences of the model parameters $\alpha$, $\phi$, $S_c$ and $S_w$ on $\Lambda_{rel}$ and $k_{rel}$. The proposed models for $\Lambda$, $\Lambda_{rel}$, $\sigma_{rel}$, $k$ and $k_{rel}$ are successfully validated using experimental data and previous models available in literature. The proposed method permits to estimate the permeability and the relative permeability directly from electrical conductivity measurements, thus opening new-avenues for the remote characterization of partially saturated media. We believe that this new model will prove useful for various characterization and modelling applications from reservoir ($CO_2$ or hydrogen storage) to vadose zone studies.

## ACKNOWLEDGMENTS

The authors strongly thank the Editor Jana Börner, Assistant Editor Louise Alexander and the reviews of Prof Konstantin Titov and an anonymous reviewer for their careful assessment of our work and their constructive comments and suggestions. This research is funded by Thuyloi University Foundation for Science and Technology under grant number TLU.STF.23-09.

## DATA AVAILABILITY

The data underlying this paper will be shared on reasonable request to the corresponding author.

## REFERENCES

Alexander, L. & Skaggs, R. W., 1987. Predicting unsaturated hydraulic conductivity from soil texture, *J. Irrigat. Drain. Eng.,* **113**(2), 184–197.

Amente, G., Baker, J. & Reece, C., 2000. Estimation of soil solution electrical conductivity from bulk soil electrical conductivity in sandy soils, *Soil Sci. Soc. Am. J.,* **64**(6), 1931–1939.

Archie, G.E., 1942. The electrical resistivity log as an aid in determining some reservoir characteristics, *Petrol. Trans. AIME,* **146,** 54–62.

Bachu, S., 2013. Drainage and imbibition $CO_2$/brine relative permeability curves at in situ conditions for sandstone formations in western Canada, *Ener. Proc.,* **37,** 4428–4436.

Banavar, J.R. & Johnson, D.L., 1987. Characteristic pore sizes and transport in porous media, *Phys. Rev. B,* **35**(13), doi:10.1103/PhysRevB.35.7283.

Bernabé, Y. & Maineult, A., 2015. 11.02 - Physics of porous media: fluid flow through porous media, in *Treatise on Geophysics,* 2nd edn, pp. 19–41, Elsevier.

Bernabé, Y., Li, M. & Maineult, A., 2010. Permeability and pore connectivity: a new model based on network simulations, *J. geophys. Res.,* **115**(B10), doi:10.1029/2010JB007444.

Bernabé, Y., Li, M., Tang, Y.-B. & Evans, B., 2016. Pore space connectivity and the transport properties of rocks, *Oil Gas Sci. Technol. – Rev. IFP Energies nouvelles,* **71**(4), doi:10.2516/ogst/2015037.

Binley, A., Winship, P., West, L., Pokar, M. & Middleton, R., 2002. Seasonal variation of moisture content in unsaturated sandstone inferred from borehole radar and resistivity profiles, *J. Hydrol.,* **267**(3), 160–172.

Brovelli, A., Cassiani, G., Dalla, E., Bergamini, F., Pitea, D. & Binley, A.M., 2005. Electrical properties of partially saturated sandstones: Novel computational approach with hydrogeophysical applications, *Water Resour. Res.,* **41**(8), doi:10.1029/2004WR003628.

Brown, J.D. & Heuvelink, G.B., 2006. Assessing uncertainty propagation through physically based models of soil water flow and solute transport, in *Encyclopedia of Hydrological Sciences,* Part 6, Chapter 79, ed. Anderson, M.G., John Wiley & Sons, Ltd.

Burdine, N., 1953. Relative permeability calculations from pore size distribution data, *J. Petrol. Technol.,* **5**(03), 71–78.

Bussian, A.E., 1983. Electrical conductance in a porous medium, *Geophysics,* **48**(9), 1258–1268.

Butler, D.B. & Knight, R.J., 1998. Electrical conductivity of steam-flooded, clay-bearing geologic materials, *Geophysics,* **63**(4), 1137–1149.

Cai, J.C., Hu, X.Y., Standnes, D.C. & You, L.J., 2012. An analytical model for spontaneous imbibition in fractal porous media including gravity, *Coll. Surf., A,* **414,** 228–233.

Campbell, G.S., 1974. A simple method for determining unsaturated conductivity from moisture retention data, *Soil Sci.,* **117**(6), 311–314.

Collini, H. & Jackson, M.D., 2022. Relationship between zeta potential and wettability in porous media: Insights from a simple bundle of capillary tubes model, *J. Coll. Interf. Sci.,* **608,** 605–621.

Corbeanu, R., McMechan, G.A., Szerbiak, R.B. & Soegaard, K., 2002. Prediction of 3-D fluid permeability and mudstone distributions from ground-penetrating radar (GPR) attributes: example from the Cretaceous Ferron sandstone member, east-central Utah, *Geophysics,* **67**(5), 1495–1504.

Daigle, H., 2016. Application of critical path analysis for permeability prediction in natural porous media, *Adv. Water Resour.,* **96,** 43–54.

Dalla, E., Cassiani, G., Brovelli, A. & Pitea, D., 2004. Electrical conductivity of unsaturated porous media: pore-scale model and comparison with laboratory data, *Geophys. Res. Lett.,* **31**(5), doi:10.1029/2003GL019170.

David, C., Gueguen, Y. & Pampoukis, G., 1990. Effective medium theory and network theory applied to the transport properties of rock, *J. geophys. Res.,* **95**(B5), 6993–7005.

Devlin, J.F., 2015. Hydrogeosievexl: an excel-based tool to estimate hydraulic conductivity from grain-size analysis, *Hydrogeol. J.,* **23,** 837–844.

Doussan, C. & Ruy, S., 2009. Prediction of unsaturated soil hydraulic conductivity with electrical conductivity, *Water Resour. Res.,* **45**(10), doi:10.1029/2008WR007309.

Doyen, P.M., 1988. Permeability, conductivity, and pore geometry of sandstone, *J. geophys. Res.,* **93**(B7), 7729–7740.

Fredlund, D.G. & Xing, A., 1994. Equations for the soil-water characteristic curve, *Can. Geotech. J.,* **31**(4), 521–532.

Friedman, S. & Seaton, N., 1998. Critical path analysis of the relationship between permeability and electrical conductivity of three-dimensional pore networks, *Water Resour. Res.,* **34,** 1703–1710.

Friedman, S.P., 2005. Soil properties influencing apparent electrical conductivity: a review, *Comput. Electr. Agric.,* **46**(1), 45–70.

Fu, Y., Horton, R., Ren, T. & Heitman, J., 2023. An unsaturated hydraulic conductivity model based on the capillary bundle model, the Brooks-Corey model and Waxman-Smits model, *Water Resour. Res.,* **59**(6), e2022WR034186.

Ghanbarian, B., 2020. Applications of critical path analysis to uniform grain packings with narrow conductance distributions: II. Water relative permeability, *Adv. Water Resour.,* **137,** doi:10.1016/j.advwatres.2020.103524.

Ghanbarian, B. & Sahimi, M., 2017. Electrical conductivity of partially saturated packings of particles, *Transp. Porous Med.,* **118,** 1–16.

Ghanbarian, B., Hunt, A.G., Ewing, R.P. & Skinner, T.E., 2014. Universal scaling of the formation factor in porous media derived by combining percolation and effective medium theories, *Geophys. Res. Lett.,* **41**(11), 3884–3890.

Ghanbarian, B., Hunt, A.G., Skaggs, T.H. & Jarvis, N., 2017. Upscaling soil saturated hydraulic conductivity from pore throat characteristics, *Adv. Water Resour.,* **104,** 105–113.

Glover, P. W.J. & Dery, N., 2010. Streaming potential coupling coefficient of quartz glass bead packs: dependence on grain diameter, pore size, and pore throat radius, *Geophysics,* **75**(6), F225–F241.

Glover, P.W.J. & Walker, E., 2009. Grain-size to effective pore-size transformation derived from electrokinetic theory, *Geophysics,* **74**(1), E17–E29.

Guarracino, L., 2007. Estimation of saturated hydraulic conductivity ks from the van Genuchten shape parameter, *Water Resour. Res.,* **43**(11), doi:10.1029/2006WR005766.

Guarracino, L. & Jougnot, D., 2022. A fractal model for effective excess charge density in variably saturated fractured rocks, *J. geophys. Res.,* **127**(3), e2021JB022982.

Herrick, D.C. & Kennedy, W.D., 1994. Electrical efficiency—a pore geometric theory for interpreting the electrical properties of reservoir rocks, *Geophysics,* **59**(6), 918–927.

Homand, F., Giraud, A., Escoffier, S., Koriche, A. & Hoxha, D., 2004. Permeability determination of a deep argillite in saturated and partially saturated conditions, *Int. J. Heat Mass Transf.,* **47**(14), 3517–3531.

Hunt, A., 2001. Applications of percolation theory to porous media with distributed local conductances, *Adv. Water Resour.,* **24**(3), 279–307.

Hunt, A.G., 2004. Continuum percolation theory and Archie's law, *Geophys. Res. Lett.,* **31**(19), 1–4.

Inoue, M., imnek, J., Shiozawa, S. & Hopmans, J., 2000. Simultaneous estimation of soil hydraulic and solute transport parameters from transient infiltration experiments, *Adv. Water Resour.,* **23**(7), 677–688.

Jackson, M.D., 2008. Characterization of multiphase electrokinetic coupling using a bundle of capillary tubes model, *J. geophys. Res.,* **113**(B4), doi:10.1029/2007JB005490.

Johnson, D.L., Koplik, J. & Schwartz, L.M., 1986. New pore-size parameter characterizing transport in porous media, *Phys. Rev. Lett.,* **57,** 2564–2567.

Johnson, D.L., Plona, T.J. & Kojima, H., 1987. Probing porous media with 1st sound, 2nd sound, 4th sound, and 3rd sound, *AIP Confe. Proc.,* **154**(1), 243–277.

Jougnot, D., Revil, A., Lu, N. & Wayllace, A., 2010. Transport properties of the Callovo-Oxfordian clay rock under partially saturated conditions, *Water Resour. Res.,* **46**(8), doi:10.1029/2009WR008552.

Kowalsky, M.B., Finsterle, S. & Rubin, Y., 2004. Estimating flow parameter distributions using ground-penetrating radar and hydrological measurements during transient flow in the Vadose Zone, *Adv. Water Resour.,* **27**(6), 583–599.

Kozeny, J., 1927. Ber kapillare leitung des wassers im boden aufsteigversikeung und anwendung auf die bemasserung, *Math-Naturwissen-schaften,* **136,** 271–306.

Le Doussal, P., 1989. Permeability versus conductivity for porous media with wide distribution of pore sizes, *Phys. Rev. B,* **39**(7), doi:10.1103/PhysRevB.39.4816.

Li, J.X., Rezaee, R., Müller, T.M. & Sarmadivaleh, M., 2021. Pore size distribution controls dynamic permeability, *Geophys. Res. Lett.,* **48**(5), e2020GL090558.

Li, K., 2011. Interrelationship between resistivity index, capillary pressure and relative permeability, *Transp. Porous Med.,* **88,** 385–398.

Li, K. & Horne, R.N., 2006. Comparison of methods to calculate relative permeability from capillary pressure in consolidated water-wet porous media, *Water Resour. Res.,* **42**(6), doi:10.1029/2005WR004482.

Li, K. & Williams, W., 2007. Determination of capillary pressure function from resistivity data, *Transp. Porous Med.,* **67,** 1–15.

Linde, N., Binley, A., Tryggvason, A., Pedersen, L.B. & Revil, A., 2006. Improved hydrogeophysical characterization using joint inversion of cross-hole electrical resistance and ground-penetrating radar traveltime data, *Water Resour. Res.,* **42**(12), doi:10.1029/2006WR005131.

Maineult, A., Jougnot, D. & Revil, A., 2018. Variations of petrophysical properties and spectral induced polarization in response to drainage and imbibition: a study on a correlated random tube network, *Geophys. J. Int.,* **212**(2), 1398–1411.

Mandelbrot, B.B., 1982. *The Fractal Geometry of Nature,* W.H. Freeman.

Mawer, C., Knight, R. & Kitanidis, P.K., 2015. Relating relative hydraulic and electrical conductivity in the unsaturated zone, *Water Resour. Res.,* **51**(1), 599–618.

Mualem, Y., 1976. A new model for predicting the hydraulic conductivity of unsaturated porous media, *Water Resour. Res.,* **12**(3), 513–522.

Mualem, Y. & Friedman, S.P., 1991. Theoretical prediction of electrical conductivity in saturated and unsaturated soil, *Water Resour. Res.,* **27**(10), 2771–2777.

Nghia, N.V., Jougnot, D., Thanh, L.D., Van Do, P., Thuy, T. T.C., Hue, D. T.M. & Hung, N.M., 2021. Predicting water flow in fully and partially saturated porous media: a new fractal-based permeability model, *Hydrogeol. J.,* **29**(6), 2017–2031.

Niu, Q., Fratta, D. & Wang, Y.-H., 2015. The use of electrical conductivity measurements in the prediction of hydraulic conductivity of unsaturated soils, *J. Hydrol.,* **522,** 475–487.

Pachepsky, Y.A. & van Genuchten, M.T., 2011. *Pedotransfer Functions,* pp. 556–561, Springer Netherlands.

Paterson, M., 1983. The equivalent channel model for permeability and resistivity in fluid-saturated rock—a re-appraisal, *Mech. Mater.,* **2**(4), 345–352.

Pini, R. & Benson, S.M., 2013. Simultaneous determination of capillary pressure and relative permeability curves from core-flooding experiments with various fluid pairs, *Water Resour. Res.,* **49**(6), 3516–3530.

Prasad, M., 2003. Velocity-permeability relations within hydraulic units, *Geophysics,* **68**(1), 108–117.

Pride, S., 1994. Governing equations for the coupled electromagnetics and acoustics of porous media, *Phys. Rev. B,* **50**(21), 15 678–15 696.

Purvance, D.T. & Andricevic, R., 2000. On the electrical-hydraulic conductivity correlation in aquifers, *Water Resour. Res.,* **36**(10), 2905–2913.

Rembert, F., Jougnot, D. & Guarracino, L., 2020. A fractal model for the electrical conductivity of water-saturated porous media during mineral precipitation-dissolution processes, *Adv. Water Resour.,* **145,** doi:10.1016/j.advwatres.2020.103742.

Revil, A., &, 1999. Permeability of shaly sands, *Water Resour. Res.,* **35**(3), 651–662.

Revil, A. & Florsch, N., 2010. Determination of permeability from spectral induced polarization in granular media, *Geophys. J. Int.,* **181**(3), 1480–1498.

Revil, A., Barnier, G., Karaoulis, M., Sava, P., Jardani, A. & Kulessa, B., 2014. Seismoelectric coupling in unsaturated porous media: theory, petrophysics, and saturation front localization using an electroacoustic approach, *Geophys. J. Int.,* **196**(2), 867–884.

Reynolds, W. & Elrick, D., 1985. In situ measurement of field-saturated hydraulic conductivity, sorptivity, and the $\alpha$-parameter using the Guelph permeameter, *Soil Sci.,* **140**(4), 292–302.

Rezaei, M., Saey, T., Seuntjens, P., Joris, I., Boënne, W., Van Meirvenne, M. & Cornelis, W., 2016. Predicting saturated hydraulic conductivity in a sandy grassland using proximally sensed apparent electrical conductivity, *J. appl. Geophys.,* **126,** 35–41.

Roubinet, D., Irving, J. & Pezard, P.A., 2018. Relating topological and electrical properties of fractured porous media: insights into the characterization of rock fracturing, *Minerals,* **8**(1), doi:10.3390/min8010014.

Rubin, Y., Mavko, G. & Harris, J., 1992. Mapping permeability in heterogeneous aquifers using hydrologic and seismic data, *Water Resour. Res.,* **28**(7), 1809–1816.

Sahimi, M. & Mukhopadhyay, S., 1996. Scaling properties of a percolation model with long-range correlations, *Phys. Rev. E,* **54,** 3870–3880.

Sen, P., Scala, C. & Cohen, M.H., 1981a. A self-similar model for sedimentary rocks with application to the dielectric constant of fused glass beads, *J. Soil Mech. Found. Div.,* **46**(5), 781–795.

Sen, P.N., Scala, C. & Cohen, M.H., 1981b. A self-similar model for sedimentary rocks with application to the dielectric constant of fused glass beads, *Geophysics,* **46**(5), 781–795.

Slater, L. & Lesmes, D.P., 2002. Electrical-hydraulic relationships observed for unconsolidated sediments, *Water Resour. Res.,* **38**(10), 31–1.

Solazzi, S.G., Rubino, J.G., Jougnot, D. & Holliger, K., 2020. Dynamic permeability functions for partially saturated porous media, *Geophys. J. Int.,* **221**(2), 1182–1189.

Soldi, M., Guarracino, L. & Jougnot, D., 2019. An analytical effective excess charge density model to predict the streaming potential generated by unsaturated flow, *Geophys. J. Int.,* **216**(1), 380–394.

Tarantino, A., Ridley, A.M. & Toll, D.G., 2008. Field measurement of suction, water content, and water permeability, *Geotech. Geol. Eng.,* **26,** 751–782.

Thanh, L.D., Van Do, P., Van Nghia, N. & Ca, N.X., 2018. A fractal model for streaming potential coefficient in porous media, *Geophys. Prospect.,* **66**(4), 753–766.

Thanh, L.D., Jougnot, D., Van Do, P. & Van Nghia A, N., 2019. A physically based model for the electrical conductivity of water-saturated porous media, *Geophys. J. Int.,* **219**(2), 866–876.

Thanh, L.D., Jougnot, D., Do, P.V., Ca, N.X. & Hien, N.T., 2020a. A physically based model for the streaming potential coupling coefficient in partially saturated porous media, *Water,* **12**(6), doi:10.3390/w12061588.

Thanh, L.D., Jougnot, D., Van Do, P., Van Nghia A, N., Tuyen, V.P., Ca, N.X. & Hien, N.T., 2020b. A physically based model for the electrical conductivity of partially saturated porous media, *Geophys. J. Int.,* **223**(2), 993–1006.

Thanh, L.D., Van Nghia, N., Van Do, P., Du, P.T. & Jougnot, D., 2023. A unified model for the permeability, electrical conductivity and streaming potential coupling coefficient in variably saturated fractured media, *Geophys. Prospect.,* **71**(2), 279–291.

Thompson, A., Katz, A. & Krohn, C., 1987. The microgeometry and transport properties of sedimentary rock, *Adv. Phys.,* **36**(5), 625–694.

Titov, K., Kemna, A., Tarasov, A. & Vereecken, H., 2004. Induced polarization of unsaturated sands determined through time domain measurements, *Vadose Zone J.,* **3**(4), 1160–1168.

Tomasella, J. & Hodnett, M.G., 1997. Estimating unsaturated hydraulic conductivity of Brazilian soils using soil-water retention data, *Soil Sci.,* **162**(10), 703–712.

Tranter, G., Minasny, B. & McBratney, A., 2010. Estimating pedotransfer function prediction limits using fuzzy k-means with extragrades, *Soil Sci. Soc. Am. J.,* **74**(6), 1967–1975.

Tuli, A. & Hopmans, J.W., 2004. Effect of degree of fluid saturation on transport coefficients in disturbed soils, *Eur. J. Soil Sci.,* **55**(1), 147–164.

Urish, D.W., 1981. Electrical resistivity-hydraulic conductivity relationships in glacial outwash aquifers, *Water Resour. Res.,* **17**(5), 1401–1408.

Van Genuchten, M.T., 1980. A closed-form equation for predicting the hydraulic conductivity of unsaturated soils, *Soil Sci. Soc. Am. J.,* **44**(5), 892–898.

Vereecken, H., 1995. Estimating the unsaturated hydraulic conductivity from theoretical models using simple soil properties, *Geoderma,* **65**(1–2), 81–92.

Vinogradov, J., Hill, R. & Jougnot, D., 2021. Influence of pore size distribution on the electrokinetic coupling coefficient in two-phase flow conditions, *Water,* **13**(17), doi:10.3390/w13172316.

Walker, E. & Glover, P., 2010. Permeability models of porous media: characteristic length scales, scaling constants and time-dependent electrokinetic coupling, *Geophysics,* **75,** E235–E246.

Walsh, J.B. & Brace, W.F., 1984. The effect of pressure on porosity and the transport properties of rock, *J. geophys. Res.,* **89**(B11), 9425–9431.

Wei, W., Cai, J., Hu, X. & Han, Q., 2015. An electrical conductivity model for fractal porous media, *Geophys. Res. Lett.,* **42**(12), 4833–4840.

Weller, A., Slater, L., Binley, A., Nordsiek, S. & Xu, S., 2015. Permeability prediction based on induced polarization: Insights from measurements on sandstone and unconsolidated samples spanning a wide permeability range, *Geophysics,* **80**(2), D161–D173.

Wheatcraft, S.W. & Tyler, S.W., 1988. An explanation of scale-dependent dispersivity in heterogeneous aquifers using concepts of fractal geometry, *Water Resour. Res.,* **24**(4), 566–578.

Wösten, J. & Van Genuchten, M.T., 1988. Using texture and other soil properties to predict the unsaturated soil hydraulic functions, *Soil Sci. Soc. Am. J.,* **52**(6), 1762–1770.

Xu, P. & Yu, B., 2008. Developing a new form of permeability and Kozeny–Carman constant for homogeneous porous media by means of fractal geometry, *Adv. Water Resour.,* **31**(1), 74–81.

Yu, B. & Cheng, P., 2002. A fractal permeability model for bi-dispersed porous media, *Int. J. Heat Mass Transf.,* **45**(14), 2983–2993.